

Ups and downs in the X-ray emission of the colliding wind binaries HD 168112 and HD 167971[★]

G. Rauw¹, R. Blomme², Y. Nazé^{1**}, D. Volpi^{2,3}, and S. Fernandez-Vera¹

¹ Space sciences, Technologies and Astrophysics Research (STAR) Institute, Université de Liège, Allée du 6 Août, 19c, Bât B5c, 4000 Liège, Belgium

² Royal Observatory of Belgium, Ringlaan 3, 1180 Brussels, Belgium

³ Faculté Sciences de la Motricité, Université Libre de Bruxelles, Campus Erasme, Route de Lennik, 808, 1070 Anderlecht, Belgium
e-mail: g.rauw@uliege.be

ABSTRACT

Context. The long-period O-star binary system HD 168112 and the triple O-star system HD 167971 are well-known sources of non-thermal radio emission that arises from a colliding wind interaction. The wind-wind collisions in these systems should result in phase-dependent X-ray emissions. The presence of a population of relativistic electrons in the wind interaction zone could affect the properties of the X-ray emission and make it deviate from the behaviour expected for adiabatic shocks.

Aims. We investigate the X-ray emission of these systems with the goals of quantifying the fraction of the X-ray flux arising from wind interactions and determining whether these emissions follow the predictions for adiabatic wind-wind collisions.

Methods. Six X-ray observations were collected with *XMM-Newton*. Three observations were scheduled around the most recent periastron passage of HD 168112. Spectra and light curves were analysed and compared with simple predictions of model calculations for X-ray emission from colliding wind systems.

Results. The X-ray emission of HD 168112 varies as the inverse of the orbital separation, as expected for an adiabatic wind interaction zone. The relative contribution of intrinsic X-ray emission from wind-embedded shocks varies between 38% at periastron to 81% at apastron. The wind-wind collision zone remains adiabatic even around periastron passage. The X-ray emission of HD 167971 displays variations on the orbital timescale of the inner eclipsing binary. The existing data of this system do not allow us to probe variations on the timescale of the outer orbit.

Conclusions. Shock modification due to the action of relativistic electrons does not seem to be efficiently operating in the HD 168112 system. In the existing observations, a significant part of the emission of HD 167971 must arise in the inner eclipsing binary. The origin of this emission is as yet unclear.

Key words. stars: early-type – stars: individual (HD 168112) – stars: individual (HD 167971) – binaries: close – X-rays: stars – Radio continuum: stars

1. Introduction

Though massive OB stars are rare objects, they are nonetheless key players in many processes in the evolution of galaxies and the Universe as a whole. One of their most remarkable properties is the existence of a powerful radiation-driven stellar wind that combines huge mass-loss rates with highly supersonic outflow velocities (e.g. Vink 2022). Most massive stars are found in binary or higher-multiplicity systems (e.g. Sana et al. 2012).

In such systems, the stellar winds of the components interact, and this interaction can impact the observational properties of these systems over a broad range of wavelengths, from X-rays into the radio domain. The head-on collision of the highly supersonic winds leads to the formation of an interaction region contained between a pair of oppositely faced, strong hydrodynamic shocks (Stevens et al. 1992). At the shock fronts, the kinetic energy normal to the shock is converted into heat, which may result in post-shock plasma temperatures of ~ 10 MK. This makes colliding wind binaries interesting targets for observations in the X-ray domain (for reviews see Rauw & Nazé 2016; Rauw 2022).

[★] Based on data collected with *XMM-Newton*, an ESA Science Mission with instruments and contributions directly funded by the ESA Member States and the USA (NASA).

^{**} F.R.S.FNRS Senior Research Associate

However, observations of large samples of massive stars indicate that very strong X-ray emission is only observed for a subset of the massive binaries (e.g. Nazé 2009).

Another observational signature of wind interactions that is relevant in the context of our present work is synchrotron non-thermal radio emission. Whilst thermal radio emission is naturally expected due to free-free emission from the stellar wind (Wright & Barlow 1975), about 15 – 25% of the massive stars in a distance-limited sample were instead found to display a clearly non-thermal radio spectrum (Abbott et al. 1984; Biegging et al. 1989). This synchrotron emission reveals the presence of a population of relativistic electrons inside the stellar winds. Theoretical models of synchrotron emission from single O-type stars were unable to explain the observed non-thermal radio emission (van Loo et al. 2005). Intense optical spectroscopic monitoring or interferometric surveys of these non-thermal radio emitter massive stars unveiled the binary or higher-multiplicity nature of these objects (e.g. Dougherty & Williams 2000; Nazé et al. 2010; Sana et al. 2014; Rauw et al. 2016). In colliding wind binaries, relativistic electrons are accelerated via the diffusive shock acceleration process at the strong hydrodynamic shocks between the stellar winds of the binary components (e.g. Reiterberger et al. 2014; Pittard et al. 2021, and references therein).

The young open cluster NGC 6604 (Reipurth 2008) hosts two O-type systems (HD 167971 and HD 168112) that are prominent non-thermal radio emitters and display a relatively strong X-ray emission (Biegging et al. 1989; De Becker et al. 2004; Blomme et al. 2005; De Becker et al. 2005; Blomme et al. 2007).

HD 167971 (MY Ser) is a triple system consisting of a close eclipsing inner binary (Leitherer et al. 1987; Davidge & Forbes 1988; Mayer et al. 2010; Ibanoglu et al. 2013) with an orbital period of 3.32 days (Ibanoglu et al. 2013, and references therein). The presence of a third component has been known for quite some time (Leitherer et al. 1987; Davidge & Forbes 1988). Maíz Apellániz et al. (2019) classified the components of the eclipsing binary as O4/5 If + O4/5 V-III and assigned an O8 Iaf spectral type to the tertiary component. However, the physical link between the inner binary and the third star was unclear at first. Blomme et al. (2007) analysed the existing radio observations of HD 167971, finding a timescale of variation of about 20 years, which they suggested is the orbital period of the third component. Multi-epoch interferometry allowed the gravitational link between the third star and the inner binary to be established (De Becker et al. 2012; Le Bouquin et al. 2017). From the light-time effect affecting the times of minimum light of MY Ser, Ibanoglu et al. (2013) inferred a period of 21.2 ± 0.7 yr and an eccentricity of 0.53 ± 0.05 for the outer orbit of the triple system. Based on interferometric measurements, Le Bouquin et al. (2017) derived a similar period of 7803 ± 540 d ($= 21.4 \pm 1.5$ yr) and an eccentricity of 0.44 ± 0.02 for the outer orbit.

Confirmation of binarity has been slower in the case of HD 168112. Based on the temporal variations in the radio flux, Blomme et al. (2005) suggested a likely orbital period of 1.4 yr. The first direct evidence for binarity came from Very Large Telescope Interferometer (VLTI) interferometry: Sana et al. (2014) detected a near-equal brightness companion ($\Delta m_H = 0.17$ mag) at a separation of 3.33 mas (corresponding to a physical separation of 6.7 AU for a distance of 2 kpc). Based on partially de-blended lines, Maíz Apellániz et al. (2019) assigned the spectral type O4.5 III(f) to the primary and O5.5 IV((f)) to the secondary¹. Quite recently, two groups independently inferred full consolidated orbital solutions for HD 168112 (Putkuri et al. 2023; Blomme et al. 2024). These radial velocity solutions yield a 514 d ($= 1.4$ yr) orbital period and reveal two nearly equal-mass stars in a highly eccentric orbit ($e \sim 0.74 - 0.75$). According to these orbital solutions, HD 168112 went through its periastron in March 2023. We monitored this event by means of three coordinated *XMM-Newton* and *Karl G. Jansky* Very Large Array (VLA) observations in the X-ray and radio domains, respectively. In the present paper, we analyse the X-ray data in light of our current knowledge of HD 168112 and HD 167971. The new radio observations of HD 168112 are discussed in detail in Blomme et al. (2024).

2. Observations and data processing

2.1. X-ray observations

Our targets were observed six times with the *XMM-Newton* satellite (Jansen et al. 2001), which carries three mirror modules that focus X-rays onto three European Photon Imaging Cameras (EPIC; Turner et al. 2001; Strüder et al. 2001) and two Reflection Grating Spectrometer (RGS; den Herder et al. 2001) instruments (RGS1 and RGS2). Two of the EPIC instruments use Metal Oxide Semiconductor (MOS; Turner et al. 2001) charge-coupled

¹ These classifications were revised to O4.5 IV((f)) + O5.5 V(n)((f)) by Putkuri et al. (2023).

device (CCD) arrays whilst the third camera uses a p-n junction CCD (pn; Strüder et al. 2001).

Under favourable spacecraft orientations, HD 168112 and HD 167971 fall into the same field of view of at least two EPIC cameras. This was the case for all our observations. However, RGS spectra are only available for the source located on-axis. During the first two observations, none of the stars was positioned on-axis. During the third observation, HD 167971 was observed on-axis, whilst HD 168112 was positioned on-axis for the three most recent observations. All EPIC observations were taken with the cameras operating in full frame mode; the thick filter was used to reject optical and UV radiation from the targets except for observation 3, for which the medium filter was used. Table 1 provides a journal of the *XMM-Newton* observations. The scheduling of the three most-recent observations was optimised to sample orbital phases around HD 168112's periastron passage in March 2023.

We processed the data with the Science Analysis System (SAS) software version 19.1.0 using the current calibration files available in January 2024. The first and third observations were affected by soft proton background flares and we discarded the corresponding time intervals. EPIC spectra were extracted from circular regions of radius 30'' centred on the *Gaia* coordinates of the two stars. The background was evaluated over an annulus of inner radius 30'' and outer radius 50''. For observation 3, we further extracted first and second order RGS1 and RGS2 spectra of HD 167971. For the last three observations, we did the same for HD 168112.

Finally, we built background-corrected light curves of both targets over the 0.5 keV – 10.0 keV band for each of the available EPIC instruments and for each observation. For this purpose, we adopted temporal bin sizes of 100, 500 and 1000 s. The light curves were corrected to get full point spread function equivalent on-axis count rates using the `epiclccor` SAS task.

Beside the *XMM-Newton* data, we also analysed an 8.7 ks ROSAT observation (Obs. ID rp500298n00) taken with the Position Sensitive Proportional Counter (PSPC) instrument between 13 and 15 September 1993. The data were retrieved from the High Energy Astrophysics Science Archive Research Center (HEASARC). We processed these data using the `xselect` software (version 2.4c) and extracted background-corrected spectra for both targets. The source spectrum was obtained from a circular region of 50'' radius, whilst the background was extracted from an annulus with inner and outer radii of respectively 50'' and 80''. The HEASARC archive further quotes High Resolution Imager (HRI) count rates for both targets obtained during another 36.0 ksec ROSAT observation (Obs. ID rh201995n00) performed between 12 September 1995 and 9 October 1995.

2.2. Radio data

Three radio observations of HD 168112 were obtained around the March 2023 periastron passage using the VLA at the National Radio Astronomy Observatory (NRAO²). These observations are part of our coordinated *XMM-Newton* and VLA monitoring. Data were acquired on three dates (3 March, 18 March, and 5 April 2023), with each date within a few days of the *XMM-Newton* observations 4 to 6 listed in Table 1. They correspond to phases 0.969, 0.998, and 0.033 using the Blomme et al. (2024) ephemerides. Each VLA observation covers the X (3.6 cm) and C (6 cm) bands, with an on-target duration of ~ 14 minutes for

² The NRAO is a facility of the US National Science Foundation operated under cooperative agreement by Associated Universities, Inc.

Table 1. *XMM-Newton* observations of HD 168112 and HD 167971.

Obs.	Obs. ID.	Duration (ks)	JD-2 450 000	EPIC filter	Target on axis	$\phi_{\text{HD 168112}}$		$\phi_{\text{HD 167971}}$	
						Putkuri	Blomme	ϕ_{inner}	ϕ_{outer}
1	0008820301	9.1	2372.56	Thick	–	0.096	0.063	0.49	0.697
2	0008820601	13.4	2526.78	Thick	–	0.396	0.364	0.92	0.717
3	0740990101	23.8	6909.73	Medium	HD 167971	0.931	0.921	0.45	0.278
4	0920040401	12.5	10009.81	Thick	HD 168112	0.968	0.974	0.75	0.676
5	0920040501	11.5	10025.98	Thick	HD 168112	0.000	0.006	0.62	0.678
6	0920040601	11.5	10042.45	Thick	HD 168112	0.032	0.038	0.58	0.680

Notes. The durations indicated in the third column correspond to the effective exposure time of the EPIC-MOS camera (i.e. after removing the time interval affected by a flare in the first and third observation). The Julian day given in column 4 is evaluated at mid-exposure. The last four columns yield the orbital phases respectively for HD 168112 (Putkuri et al. 2023 and Blomme et al. 2024), the eclipsing inner binary of HD 167971 (Ibanoglu et al. 2013) and the orbit of the outer component of HD 167971 (Le Bouquin et al. 2017).

each band. More details about these radio observations and their data processing are presented in Blomme et al. (2024).

3. X-ray data analysis

3.1. Light curves

We performed χ^2 tests to assess the significance of short-term variability against the hypothesis of a constant count rate. We further tested the significance of several possible trends: a linear time dependence, or a quadratic trend with time. Testing the null hypothesis of a constant count rate, we found that the majority of the light curves do not display any significant variability, that is to say, the significance level SL of the null hypothesis remains above 5%. A handful of light curves with time bins of 100 s have $SL < 5\%$, but their 1 ks counterparts (for the same instrument during the same observation) always have $SL \gg 5\%$. Furthermore, the apparent detection of significant variations concerns only a single instrument. Indeed, light curves with 100 s time bins from the other two EPIC instruments during the same observation have $SL > 5\%$, showing that these apparent detections are statistical flukes. A few light curves are better represented by a linear or quadratic trend, but again this is not confirmed by light curves recorded by the other EPIC instruments during the same observation. We thus conclude that neither of the two binaries displays significant intra-pointing variations beyond the fluctuations consistent with Poisson noise.

3.2. Spectral fits

To characterise the spectral energy distributions of both targets in the X-ray domain, we adjusted their *XMM-Newton* spectra using version 12.9.0i of the *xspec* code (Arnaud 1996). For each observation, all available spectra (EPIC and RGS) of a given target were fitted simultaneously. To avoid biases due to the fact that the RGS spectra exist only for a subset of the observations, we also performed fittings of the sole EPIC data for those observations where RGS data were available. We found that the EPIC only and EPIC+RGS spectral fits were fully consistent with each other and all model parameters overlapped well within their error bars.

High-resolution X-ray spectra of O-type stars unveil a wealth of emission lines of highly ionised species. These spectra indicate that the X-ray emission arises from an optically thin thermal

plasma. We thus tested models of the kind

$$\text{TBabs} * \text{phabs} * \sum_{i=1}^N \text{apec}(kT_i). \quad (1)$$

The *apec* components yield the X-ray emission of collisionally ionised, optically thin thermal plasma components (Smith & Brickhouse 2001). In our models we used $N = 2$ and $N = 3$ as we found that a single temperature plasma model ($N = 1$) was unable to provide a good fit over the full energy range of the data. The *TBabs* model (Wilms et al. 2000) accounts for the photoelectric absorption by the interstellar medium (ISM) along our sightline towards the source. For HD 167971, Gudennavar et al. (2012) quoted a total interstellar neutral hydrogen column density of $(5.4 \pm 4.0) \times 10^{21} \text{ cm}^{-2}$. Whilst the error bar on this column density is large, we note that the value is fully consistent with the mean relation between $N(\text{H I})$ and $E(B - V)$. Indeed, for $E(B - V) = 0.87$, the Bohlin et al. (1978) relation yields $5.0 \times 10^{21} \text{ cm}^{-2}$, whilst the relation of Gudennavar et al. (2012) yields $5.3 \times 10^{21} \text{ cm}^{-2}$. In our models, we thus fixed the ISM column of HD 167971 to $5.15 \times 10^{21} \text{ cm}^{-2}$, which is the mean of the values obtained with the two $N(\text{H I}) - E(B - V)$ relations. For HD 168112, no direct measurements of the neutral hydrogen column are available. For $E(B - V) = 0.97$ the same relations yield columns of $5.6 \times 10^{21} \text{ cm}^{-2}$ and $5.9 \times 10^{21} \text{ cm}^{-2}$. In our fits, we therefore fixed the ISM column of HD 168112 to $5.75 \times 10^{21} \text{ cm}^{-2}$. Our spectral models further included a *phabs* multiplicative absorption component to account for additional photoelectric absorption within the stellar winds, with the corresponding hydrogen column density considered a free parameter of the model. We stress here that the main objective of our spectral fits is to obtain a good description of the overall X-ray spectral energy distribution. Whilst the model parameters likely reflect the mean properties of the plasma, they should not be over-interpreted, especially because of the model degeneracies between the action of absorbing material and the intrinsic hardness of the emitting plasma. This remark is especially relevant for the lower temperature plasma component and explains the large error bars on the normalisation of the softest *apec* component. However, since this component contributes only a small fraction of the overall flux, this large error has little impact on the flux derivation.

3.2.1. HD 168112

The X-ray spectra of HD 168112 can be reasonably well described by a two-temperature (2-T) plasma model. The above-mentioned degeneracy between wind column density and plasma

temperature is especially apparent when comparing the parameters of observation 2 with those of the other exposures. Adding a third plasma component significantly improves the quality of the fits for the most recent exposures that have the best statistics (see Table 2). The improvement is marginal for observations 1 and 2, which have the poorest statistics. Since the 3-T fits yield a better adjustment of the overall spectral energy distribution, we use the flux values inferred from those fits in what follows. The total X-ray flux of HD 168112 exhibits highly significant variations between the various observations (see Table 2 and Fig. 1). This result is independent of the model (2-T or 3-T), although, as indicated before, the 3-T models better represent the true flux of the source.

Owing to the smaller energy range covered by the ROSAT-PSPC instrument, the PSPC spectrum was fitted using a 1-T model. Assuming the same set of 1-T model parameters (except for the normalisation) describes the properties of the source during the ROSAT-HRI observation, we used the HEASARC WebPIMMS tool³ to convert the HRI count rates into fluxes in the 0.5 keV – 1.0 keV and 1.0 keV – 2.0 keV energy domains.

As outlined in Sect. 1, HD 168112 and HD 167971 are known as synchrotron non-thermal radio emitters. This synchrotron emission reflects the presence of a population of relativistic electrons accelerated by diffusive shock acceleration in the colliding wind region. In principle, inverse Compton (IC) scattering of stellar UV photons by those relativistic electrons could result in a non-thermal X-ray emission with a power law photon index $\Gamma = \frac{n+1}{2}$ where n is the index of the energy distribution of the relativistic electrons (Chen & White 1991). To check for the existence of such a non-thermal X-ray emission, we adjusted models of the kind

$$\text{TBabs} * \text{phabs} * \left(\sum_{i=1}^2 \text{apec}(kT_i) + \text{power} \right), \quad (2)$$

where the power component stands for a non-thermal emission described by a power law relation. This model usually resulted in fits of very similar quality as for the 3-T thermal plasma model. The best-fit photon index of the power law turned out to be highly variable between exposures, changing from 2.2 to 6.9. These indices differ significantly from the value expected for a population of relativistic electrons ($\Gamma \sim 1.5$) if the shocks responsible for the acceleration have the usual compression ratio ~ 4 . Moreover, their erratic variations further indicate that there currently is no clear evidence for the existence of a non-thermal component in the X-ray emission of HD 168112. Moreover, the best quality EPIC-pn spectra (observations 4, 5 and 6) display an Fe xxv line at 6.7 keV, which is a clear indication that the harder X-ray emission arises inside a very hot thermal plasma. We come back to this point in Sect. 4.1.

3.2.2. HD 167971

HD 167971 is a few times brighter in X-rays than HD 168112. Its X-ray spectra are again reasonably well described by means of 2-T plasma models. However, including a third plasma component significantly improves the quality of the fits for the majority of the exposures (see Table 3). We observe significant variations in the total flux between the different exposures, although they are of lower amplitude than in the case of HD 168112 (see Table 3). The highest quality EPIC-pn spectrum (observation 3) displays a clear Fe xxv emission near 6.7 keV consistent with a rather high

plasma temperature. The ROSAT data were analysed in the same way as for HD 168112.

As for HD 168112, we also adjusted models including a power law component as of Eq. 2. Compared to the 3-T models, the 2-T + power law model resulted in a slight improvement of the quality of the fits in 4 cases out of 6. We found again best-fit photon indices that were quite different from the expected value of 1.5. For all observations, except the third one, Γ was found to be in the range 2.6 – 3.4. For the third observation, the best agreement with the data was achieved for $\Gamma = 7.9$. Again, we conclude that there is currently no evidence for the existence of a genuine non-thermal component in the X-ray emission of HD 167971. We return to this point in Sect. 4.2.

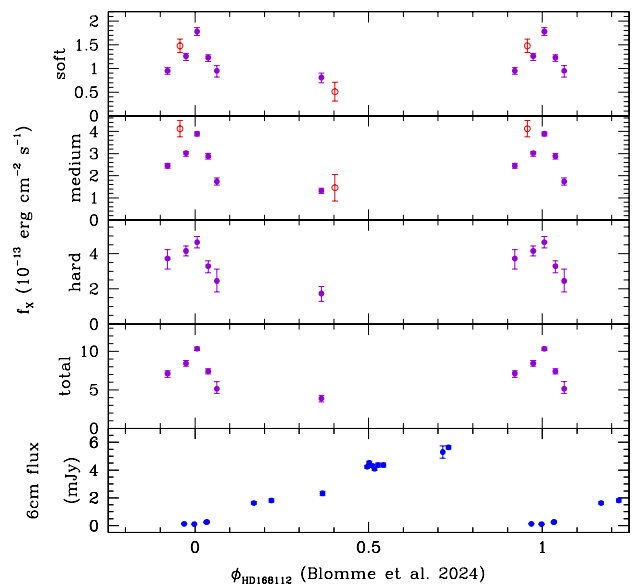


Fig. 1. Observed X-ray and radio flux of HD 168112 as a function of the orbital phase evaluated with the ephemerides of Blomme et al. (2024). The top four panels correspond to the different energy bands in the X-ray domain: soft (0.5 keV – 1.0 keV), medium (1.0 keV – 2.0 keV), hard (2.0 keV – 4.0 keV), and total (0.5 keV – 10 keV). Violet filled symbols correspond to *XMM-Newton* observations, and the red open circles indicate the ROSAT data. The error bars on the X-ray fluxes correspond to the 90% confidence intervals. The bottom panel presents the 6 cm radio flux data from Blomme et al. (2005).

4. Discussion

The properties of the hot plasma in a colliding wind interaction zone depend strongly on the efficiency of radiative cooling (Stevens et al. 1992). If the plasma density is high, collisional recombinations will be frequent resulting in a fast radiative cooling. As a result, the plasma temperature drops rapidly before the material escapes the system. This situation applies notably to massive binaries with short orbital periods such as the inner eclipsing binary in HD 167971. On the contrary, in wide massive binaries, such as HD 168112 or the outer system of HD 167971, the density of the plasma in the post-shock region of the colliding winds interaction is comparatively low. As a result, radiative cooling should be negligible and the hot shocked plasma only cools adiabatically. Under these circumstances, the X-ray luminosity is expected to scale with $1/r$ where r is the instantaneous orbital separation between the stars (Stevens et al. 1992; Pittard & Dawson 2018).

³ <http://heasarc.gsfc.nasa.gov/cgi-bin/Tools/w3pimms/w3pimms.pl>

Table 2. Fits of the X-ray spectra of HD 168112 using 3-T plasma models.

Obs.	Instruments	N_{H} (10^{22} cm^{-2})	kT_1 (keV)	norm ₁ (cm^{-5})	kT_2 (keV)	norm ₂ (cm^{-5})	kT_3 (keV)	norm ₃ (cm^{-5})	χ^2_{ν}	d.o.f.	f_X (0.5 - 10 keV) ($10^{-14} \text{ erg cm}^{-2} \text{ s}^{-1}$)
1	MOS1+2	$0.54^{+0.18}_{-0.20}$	$0.20^{+0.13}_{-0.15}$	$(4.4^{+157.9}_{-3.6}) 10^{-3}$	$0.56^{+0.22}_{-0.19}$	$(7.3^{+4.0}_{-6.1}) 10^{-4}$	≥ 2.8	$(2.3^{+1.2}_{-0.8}) 10^{-4}$	0.94	66	$51.4^{+9.4}_{-5.9}$
2	MOS1+2	$0.26^{+0.20}_{-0.20}$	$0.14^{+0.83}_{-0.14}$	$(2.7^{+297.5}_{-2.6}) 10^{-3}$	$0.60^{+0.08}_{-0.12}$	$(4.5^{+2.2}_{-1.1}) 10^{-4}$	≥ 2.5	$(1.9^{+0.8}_{-0.7}) 10^{-4}$	0.76	61	$38.7^{+2.7}_{-4.5}$
3	EPIC	$0.59^{+0.13}_{-0.27}$	$0.26^{+0.05}_{-0.03}$	$(4.4^{+4.7}_{-3.5}) 10^{-3}$	$1.26^{+0.20}_{-0.38}$	$(5.1^{+1.3}_{-2.4}) 10^{-4}$	≥ 2.7	$(2.5^{+2.8}_{-0.8}) 10^{-4}$	0.85	162	71.2 ± 4.9
4	EPIC+RGS	$0.28^{+0.20}_{-0.20}$	$0.33^{+0.12}_{-0.05}$	$(9.4^{+19.4}_{-7.0}) 10^{-4}$	$0.94^{+0.09}_{-0.08}$	$(3.9^{+1.1}_{-1.0}) 10^{-4}$	$2.9^{+0.5}_{-0.4}$	$(5.9^{+0.8}_{-0.9}) 10^{-4}$	0.96	451	84.3 ± 3.7
5	EPIC+RGS	$0.33^{+0.11}_{-0.13}$	$0.31^{+0.09}_{-0.03}$	$(2.0^{+1.4}_{-1.2}) 10^{-3}$	$0.98^{+0.07}_{-0.07}$	$(5.8^{+1.4}_{-1.3}) 10^{-4}$	$2.9^{+0.6}_{-0.4}$	$(6.3^{+1.2}_{-1.0}) 10^{-4}$	1.11	493	103.1 ± 2.3
6	EPIC+RGS	$0.52^{+0.11}_{-0.11}$	$0.30^{+0.08}_{-0.06}$	$(2.2^{+2.7}_{-1.1}) 10^{-3}$	$0.76^{+0.16}_{-0.07}$	$(6.5^{+3.0}_{-2.2}) 10^{-4}$	$3.2^{+1.1}_{-0.6}$	$(4.3^{+0.9}_{-0.9}) 10^{-4}$	1.03	414	74.0 ± 3.3

Notes. The model was defined according to Eq. (1) with $N = 3$. The ISM column was fixed to $5.75 \times 10^{21} \text{ cm}^{-2}$. Abundances were fixed to solar following Asplund et al. (2009). The plasma normalisation parameters are equal to $\frac{10^{-14}}{4\pi D^2} \int n_e n_H dV$ in units cm^{-5} with D the distance of the source and $\int n_e n_H dV$ the emission measure of the plasma. The last column yields the observed flux in the 0.5 – 10 keV band. The quoted errors correspond to the 90% confidence intervals. The uncertainties on the observed fluxes were evaluated using the `cflux` command of the `xspec` software.

Table 3. Fits of the X-ray spectra of HD 167971 using 3-T plasma models.

Obs.	Instruments	N_{H} (10^{22} cm^{-2})	kT_1 (keV)	norm ₁ (cm^{-5})	kT_2 (keV)	norm ₂ (cm^{-5})	kT_3 (keV)	norm ₃ (cm^{-5})	χ^2_{ν}	d.o.f.	f_X (0.5 - 10 keV) ($10^{-13} \text{ erg cm}^{-2} \text{ s}^{-1}$)
1	MOS1+2	$0.72^{+0.11}_{-0.12}$	$0.31^{+0.07}_{-0.03}$	$(11.9^{+7.9}_{-6.0}) 10^{-3}$	$0.86^{+0.12}_{-0.15}$	$(12.8^{+7.7}_{-5.5}) 10^{-4}$	$3.0^{+2.6}_{-0.9}$	$(6.5^{+3.1}_{-2.6}) 10^{-4}$	0.85	111	16.6 ± 1.1
2	EPIC	$0.64^{+0.06}_{-0.07}$	$0.30^{+0.03}_{-0.02}$	$(8.6^{+3.3}_{-2.6}) 10^{-3}$	$0.98^{+0.07}_{-0.07}$	$(12.9^{+2.6}_{-2.6}) 10^{-4}$	$3.1^{+2.8}_{-0.8}$	$(4.4^{+2.1}_{-1.8}) 10^{-4}$	1.11	231	14.1 ± 0.7
3	EPIC+RGS	$0.60^{+0.04}_{-0.04}$	$0.30^{+0.02}_{-0.01}$	$(6.3^{+1.6}_{-1.4}) 10^{-3}$	$0.81^{+0.04}_{-0.03}$	$(16.9^{+2.3}_{-2.2}) 10^{-4}$	$2.0^{+0.2}_{-0.1}$	$(8.4^{+1.0}_{-1.1}) 10^{-4}$	1.13	967	15.8 ± 0.4
4	EPIC	$0.53^{+0.09}_{-0.09}$	$0.31^{+0.08}_{-0.03}$	$(6.6^{+4.4}_{-3.3}) 10^{-3}$	$0.84^{+0.12}_{-0.08}$	$(16.6^{+6.0}_{-2.9}) 10^{-4}$	$1.9^{+0.5}_{-0.3}$	$(10.8^{+2.6}_{-2.7}) 10^{-4}$	1.09	180	19.1 ± 0.9
5	EPIC	$0.40^{+0.09}_{-0.15}$	$0.15^{+0.22}_{-0.06}$	$(10.2^{+63.6}_{-7.4}) 10^{-3}$	$0.65^{+0.33}_{-0.05}$	$(21.0^{+6.1}_{-7.7}) 10^{-4}$	$1.3^{+0.1}_{-0.1}$	$(19.3^{+2.4}_{-4.6}) 10^{-4}$	1.22	186	20.0 ± 0.9
6	EPIC	$0.47^{+0.16}_{-0.17}$	$0.34^{+0.21}_{-0.07}$	$(3.9^{+7.5}_{-2.9}) 10^{-3}$	$0.79^{+0.13}_{-0.09}$	$(16.3^{+7.2}_{-6.4}) 10^{-4}$	$1.9^{+0.5}_{-0.3}$	$(12.5^{+3.3}_{-3.1}) 10^{-4}$	1.15	143	19.1 ± 0.9

Notes. Same as Table 2, but the ISM column was here fixed to $5.15 \times 10^{21} \text{ cm}^{-2}$. For observation 5, a few deviating energy bins of the EPIC-pn spectrum below 0.4 keV were excluded from the fitting procedure.

The efficiency of radiative cooling is usually quantified through the ratio between the radiative cooling time and the escape time from the shock region $\chi = \frac{t_{\text{cool}}}{t_{\text{esc}}} = \frac{v_{\infty}^4 r}{\dot{M}}$ (Stevens et al. 1992). Here r stands for the instantaneous orbital separation of the stars, \dot{M} and v_{∞} are the wind mass-loss rate and wind terminal velocity (assuming the wind has the time to accelerate to its terminal velocity before the collision). Adopting the spectral types inferred by Maíz Apellániz et al. (2019) or those quoted by Putkuri et al. (2023) along with the corresponding mass-loss rates and wind velocities from Muijres et al. (2012), we infer $\chi \geq 22$ for both shocked winds of HD 168112. This result holds at all orbital phases, with the lowest value being reached at periastron. Hence, the radiative cooling via collisional recombination should be negligible at all orbital phases.

Collisional recombination might not be the sole cooling mechanism affecting the post-shock plasma. Mackey et al. (2023) drew attention to the importance of IC cooling that can become the primary cooling mechanism notably in eccentric binary systems with large wind momentum ratios. IC cooling of the thermal electrons could make the shocked winds strongly radiative near periastron despite the fact that the Stevens et al. (1992) criterion would indicate them to be in the adiabatic regime. Mackey et al. (2023) therefore formulate a specific criterion to evaluate the importance of IC cooling: $\chi_{\text{IC}} = \frac{1.61 \chi_{12}^{\text{stag}} v_8}{L_5}$.

Here χ_{12}^{stag} stands for the distance from the centre of the star to the shock in units 10^{12} cm , v_8 is the pre-shock velocity in units 1000 km s^{-1} and L_5 the bolometric luminosity of the star in units $10^5 L_{\odot}$. If $\chi_{\text{IC}} < 1$, then IC cooling makes the shock radiative. Applying this criterion to HD 168112 at periastron, we infer $\chi_{\text{IC}} \geq 8$ for both components of the system. Hence, we conclude that both criteria suggest that the wind interaction zone remains in the adiabatic regime all around the orbital cycle.

Applying the same calculations to the inner binary of HD 167971 yields $\chi = 3.2 (v/v_{\infty})^4$ and $\chi_{\text{IC}} = 0.9 (v/v_{\infty})$. Because of the proximity of the two stars and their mutual radiation fields, their winds do not accelerate to v_{∞} before they collide. Assuming that they reach $v_{\infty}/2$, which seems rather optimistic, we would find $\chi \approx 0.2$ and $\chi_{\text{IC}} \approx 0.4$, indicating that the shocked winds should be in the radiative regime. For the wind interaction between the inner binary and the tertiary component, the cooling parameters vary with phase because of the changing orbital separation. In this case, we find $\chi \geq 295$ and $\chi_{\text{IC}} \geq 75$.

Wide eccentric binaries offer an ideal testbed for the theory of adiabatic wind interactions, and more specifically for the predicted $1/r$ dependence of the X-ray flux. Evidence for such a behaviour was found in several O + O and Wolf-Rayet (WR) + O binaries (e.g. Nazé et al. 2012; Pandey et al. 2014; Gosset & Nazé 2016), but strong deviations from this simple expectation were observed in other systems among which the long-period

(8 – 9 years) binaries 9 Sgr (Rauw et al. 2016) and WR 140 (Zhekov 2021). At first sight, some departures from the $1/r$ scaling could be due to radiative inhibition or braking (Stevens & Pollock 1994; Gayley et al. 1997). However, the efficiency of this mechanism is strongly reduced by the wide separation between the stars even around periastron passage. For 9 Sgr and WR 140, part of the explanation may reside instead in the fact that both systems are non-thermal radio sources and, thus, host relativistic electrons in their wind interaction zone. Indeed, the pressure that relativistic particles, accelerated by the diffusive shock acceleration mechanism, exert on the pre-shock flow should indeed lead to shock modification (Pittard & Dougherty 2006). Both systems investigated in the present study display non-thermal radio emission indicating the presence of populations of relativistic electrons. Both systems feature a wind-wind collision that arises in a highly eccentric orbit with a wide orbital separation. They are thus ideal targets to investigate the impact of shock modification on the X-ray emission of colliding wind systems.

4.1. Colliding winds in HD 168112

Figure 1 illustrates the variability of the X-ray and radio fluxes of HD 168112 with orbital phase computed using the ephemerides of Blomme et al. (2024). Quite similar results are obtained if we use the ephemerides of Putkuri et al. (2023), although there is a small shift in phase⁴ (see Table 1). The X-ray flux displays a significant increase, by a factor of 2 to 3, around periastron passage. Whilst this increase is observed in all energy bands, the strongest variations (by a factor of 3.0) occur in the medium energy band, whilst the soft energy band displays the lowest increase (by a factor of 2.2).

Figure 2 illustrates the X-ray flux in the 0.5 – 10 keV energy band, corrected for absorption by the ISM, as a function of the ratio a/r computed from the orbital solution of Blomme et al. (2024). Here a stands for the orbital semi-major axis, whilst r is the instantaneous orbital separation. The straight line yields a least square fit to these data given by

$$f_X(10^{-13} \text{ erg cm}^{-2} \text{ s}^{-1}) = (3.16 \pm 0.42)(a/r) + (7.75 \pm 1.05). \quad (3)$$

Using instead the Putkuri et al. (2023) orbital solution yields a very similar relation with the numerical values of 3.30 ± 0.45 and 7.41 ± 1.10 . The best-fit relation of Eq. 3 is illustrated in Fig. 3 along with the phase dependence of r/a and of the position angle θ defined as the true anomaly variation between the conjunction with the O4.5 IV primary star in front and the actual direction of the line joining the two stars. We observe no obvious dependence of the X-ray fluxes on θ , which indicates that the observed variations are not due to absorption effects.

In shorter period systems (e.g. WR 21a, $P_{\text{orb}} = 31.7$ days and Cyg OB2 #8a, $P_{\text{orb}} = 21.9$ days), the X-ray emission displays an asymmetric behaviour between phases before and after periastron (e.g. Gosset & Nazé 2016; Mossoux et al. 2020). This was attributed to disruptions of the shock at periastron, and the shock subsequently needing some time to recover as the orbital separation increased again. Our observations of HD 168112 at $\phi = 0.974$ (observation 4) and $\phi = 0.038$ (observation 6) allowed us to check for the existence of such a hysteresis-like behaviour. Table 2 clearly shows the similarity in properties of these two phases. Therefore, we find no significant evidence for such a

⁴ We focus on the results obtained with the Blomme et al. (2024) orbital solution as it contains significantly more data points around periastron passage and should thus result in better constrained orbital elements.

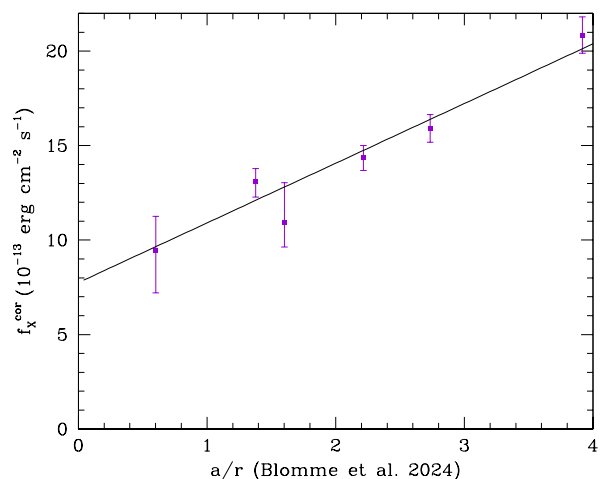


Fig. 2. X-ray flux of HD 168112 in the 0.5 keV – 10 keV energy band corrected for absorption by the ISM as a function of a/r computed according to the orbital solution from Blomme et al. (2024). The straight line corresponds to the linear fit given by Eq. 3.

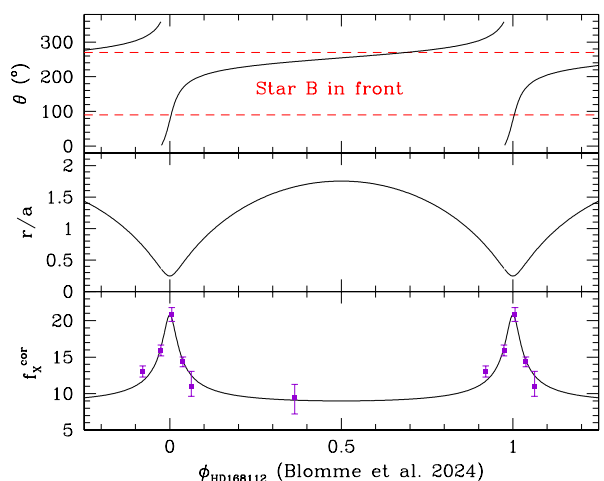


Fig. 3. Variation in the position angle (top panel) and the orbital separation (r/a) as a function of the orbital phase computed according to the orbital solution from Blomme et al. (2024). The position angle is measured in the orbital plane and is defined here as the angle between the line joining the two stars and the direction of conjunction with the primary star (labelled component A in Blomme et al. 2024) in front. Phase 0.0 corresponds to periastron passage. Bottom panel: X-ray flux of HD 168112 in the 0.5 keV – 10 keV energy band corrected for absorption by the ISM as a function of orbital phase along with the best fit $1/r$ scaling of the colliding wind X-ray emission given by Eq. 3.

phenomenon in the HD 168112 system: the variations in the X-ray flux appear rather symmetrical around periastron passage.

As described above, the presence of relativistic electrons in the wind interaction zone of HD 168112 could result in shock modification (Pittard & Dougherty 2006). This should in turn lower the X-ray luminosity (compared to the $1/r$ relation) and the post-shock temperature and, hence, the temperature of the X-ray emitting plasma (Pittard & Dougherty 2006). Figures 2 and 3 do not show any evidence for a significant deviation of the X-ray flux from the $1/r$ relation.

As outlined in Sect. 1, HD 168112 displays a non-thermal radio emission that is most likely associated with the wind inter-

action zone. De Becker et al. (2024) presented European Very Long Baseline Interferometry Network (EVN) radio observations of HD 168112 collected in November 2019 with an angular resolution of $12 \times 22 \text{ mas}^2$. The date of the EVN observations corresponds to phase $\phi = 0.598$ of HD 168112 according to the Blomme et al. (2024) ephemerides. The radio emission of HD 168112 was partially resolved and found to be elongated, consistent with the emission expected from a colliding wind interaction.

The bottom panel of Fig. 1 illustrates the variations in the observed radio emission at 6 cm wavelength (using our new VLA radio observations along with the radio light curve of Blomme et al. 2005). This radio emission displays a pronounced minimum around periastron passage. This minimum could reflect a genuine disruption of the shock around periastron passage. Indeed, if the shock were disrupted (as seen in WR 21a or Cyg OB2 #8a), the particle acceleration mechanism would be temporarily switched off, resulting in a strong attenuation of the synchrotron radio emission. However, the symmetrical variations in the X-ray flux around periastron clearly indicate that the shock is not disrupted. Instead, the most likely explanation of the radio minimum is the substantial free-free absorption by the stellar wind material. Indeed, as the stars approach periastron, the colliding wind interaction moves deeper into the optically thick winds and the synchrotron radio emission is strongly attenuated (Blomme et al. 2005). From the variations in the position angle in Fig. 3, we also see that the wind interaction zone remains partially hidden behind the radio photosphere of the secondary until about phase 0.35 and fully emerges only once the orbital separation increases as the stars approach apastron. This situation is quite reminiscent of the behaviour observed for Cyg OB2 #9 (O5-5.5 I + O3-4 III, $P_{\text{orb}} = 858.4 \text{ d}$, $e = 0.71$, Nazé et al. 2012; Blomme et al. 2013). We refer to Blomme et al. (2024) for a more extensive discussion of the radio emission of HD 168112.

The VLTI observation analysed by Sana et al. (2014) corresponds to orbital phase $\phi = 0.334$ with the Blomme et al. (2024) ephemerides. At this phase, the orbital separation amounts to $1.62 a$, and θ is equal to 241° . The third *Gaia* data release yields a parallax of $0.498 \pm 0.020 \text{ mas}$ for HD 168112. Together with the $a \sin i = 897 R_\odot$, the angular separation yields an inclination of $i \simeq 63^\circ$. Combining this inclination with the minimum masses inferred by Blomme et al. (2024), we obtain absolute masses for the two stars of 26.1 and $25.9 M_\odot$. Using instead the orbital solution of Putkuri et al. (2023), that is, $a \sin i = 1005 R_\odot$, we obtain $i \simeq 77^\circ$ and absolute masses of the two stars of 29.2 and $26.5 M_\odot$. The components of HD 168112 were classified as O4.5 IV((f)) for the primary and O5.5 V(n)((f)) for the secondary (Putkuri et al. 2023). In both cases, the absolute masses that we derive from the comparison of the orbital solutions with the interferometric measurement are lower by $\sim 25\%$ than the masses expected for stars of these spectral types (Martins et al. 2005).

The bolometric luminosities of the components were given as $\log L_{\text{bol}}/L_\odot = 5.64 \pm 0.12$ and 5.53 ± 0.08 respectively for the primary and secondary (Putkuri et al. 2023). Comparing the X-ray luminosities, evaluated from the fluxes in the $0.5 - 10 \text{ keV}$ range corrected for the interstellar absorption only, with these bolometric luminosities we find $\frac{L_X}{L_{\text{bol}}}$ of $1.5 \cdot 10^{-7}$ at apastron and $3.4 \cdot 10^{-7}$ at periastron. If we adopt instead typical bolometric magnitudes as quoted by Martins et al. (2005) for stars of equal spectral types, we obtain $\frac{L_X}{L_{\text{bol}}}$ of $1.2 \cdot 10^{-7}$ at apastron and $2.7 \cdot 10^{-7}$ at periastron.

In this context, it is interesting to consider the $\frac{L_X}{L_{\text{bol}}}$ ratio corresponding to the constant term in Eq. 3. Adopting the bolo-

metric luminosities from Putkuri et al. (2023), we find that this constant term yields $\frac{L_X}{L_{\text{bol}}} = 1.3 \cdot 10^{-7}$. This constant X-ray emission likely reflects the intrinsic emission due to wind-embedded shocks in the two stars in the binary system. Quite remarkably the associated luminosity follows very closely the canonical relation for the intrinsic emission of O-type stars (Berghöfer & Schmitt 1995; Nazé 2009). From Eq. 3, we further note that the wind-embedded shocks (i.e. the constant term in the relation) contribute between 38% (at periastron) and 81% (at apastron) of the total X-ray flux.

The presence of a population of relativistic electrons in the wind interaction region of HD 168112 further opens up the possibility that IC scattering of stellar UV photons by these relativistic electrons could result in a non-thermal X-ray or γ -ray emission (Pittard et al. 2021). Indeed, the η Car colliding wind system was detected at energies above 20 keV with the International Gamma Ray Astrophysics Laboratory (INTEGRAL) and *NuSTAR* (Leyder et al. 2010; Hamaguchi et al. 2018), and up into the GeV domain with *Agile* and *Fermi* (Farnier et al. 2011; Reitberger et al. 2015). So far all attempts to detect such a non-thermal X-ray emission over the $0.5 - 10 \text{ keV}$ band in other particle accelerating colliding wind binaries failed (e.g. Rauw et al. 2002; Mossoux et al. 2020). This indicates that any non-thermal X-ray emission must be significantly weaker than the thermal emission from the colliding winds binary, at least at energies below 10 keV .

Pittard et al. (2021) estimated that IC energy losses by relativistic electrons are important for systems with orbital separation of less than 10^{14} cm . For HD 168112, the orbital separation varies between $248 R_\odot$ ($1.73 \cdot 10^{13} \text{ cm}$) at periastron and $1766 R_\odot$ ($1.23 \cdot 10^{14} \text{ cm}$) at apastron adopting the Blomme et al. (2024) orbital elements and taking $i = 63^\circ$. Hence, IC scattering by relativistic electrons should be relevant for this system over most orbital phases, and certainly around periastron. Our spectral fitting tests including a power law component yielded photon indices that varied over a wide range and were usually quite different from the expected value of 1.5. In this context, it is interesting to note that Pittard et al. (2021) drew attention to the large variations in the spectral indices of the relativistic particles in their models of colliding wind binaries, which make the usual $N(E) \propto E^{-2}$, where $N(E)$ stands for the number of photons emitted with an energy E , too simplistic. In the energy range between 1 and 10 keV , where non-thermal emission is dominated by IC scattering, their models always predict a photon index Γ in the range 1.5 to 2 . Hence, we performed another series of spectral fittings adopting a model as given by Eq. 2, but this time keeping the photon index fixed to $\Gamma = 1.5$. These fits were of significantly poorer quality than those described in Sect. 3.2.1. Nevertheless, the normalisation of the power-law component was usually significant at the $\sim 4\sigma$ level and its intrinsic flux in the $0.5 \text{ keV} - 10 \text{ keV}$ band would be typically of order $3 \cdot 10^{-13} \text{ erg cm}^{-2} \text{ s}^{-1}$, corresponding to $\sim 10\%$ of the total intrinsic flux. However, we note that these spectral fits failed to properly reproduce the Fe xxv line at 6.7 keV , which requires a high-temperature thermal plasma (see Table 2). Therefore, we conclude that the existing data do not provide any evidence for a significant non-thermal X-ray emission in HD 168112. The above quoted flux associated with such a component is thus to be considered as a very conservative upper limit.

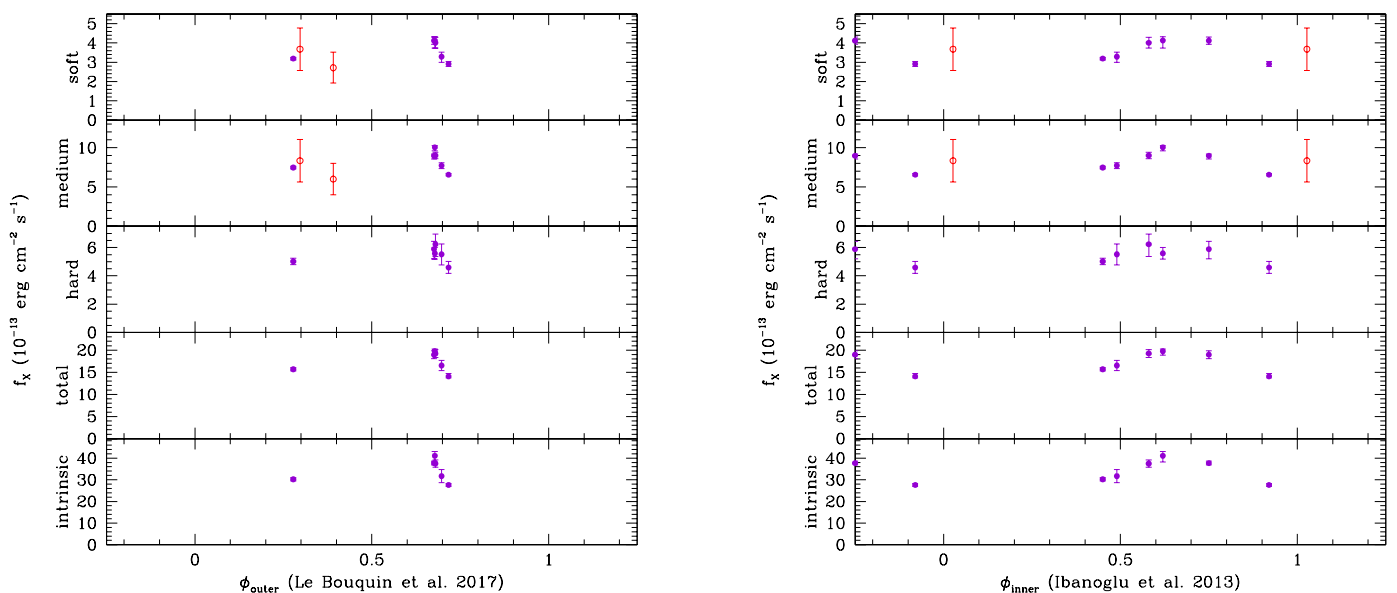


Fig. 4. Variations in the X-ray flux of HD 167971. Left panel: X-ray flux of HD 167971 as a function of the orbital phase of the tertiary component (Le Bouquin et al. 2017). Phase $\phi_{\text{outer}} = 0$ corresponds to periastron passage. The top four panels correspond to the observed X-ray flux in four different energy bands: soft (0.5 keV – 1.0 keV), medium (1.0 keV – 2.0 keV), hard (2.0 keV – 4.0 keV), and total (0.5 keV – 10 keV). Violet filled symbols indicate *XMM-Newton* data, and open red circles stand for ROSAT observations. The bottom panel yields the flux in the 0.5 keV – 10 keV band corrected for absorption by the ISM. Right panel: Same but as a function of the orbital phase of the inner eclipsing binary (Ibanoglu et al. 2013). Here $\phi_{\text{inner}} = 0$ corresponds to the primary minimum of the eclipsing binary. Because the ROSAT-HRI observation spanned nearly one month (i.e. more than eight orbital cycles) it is not shown here.

4.2. Colliding winds in HD 167971

The X-ray fluxes of HD 167971 in the 0.5 – 10 keV band corrected for the interstellar absorption range between $2.75 \cdot 10^{-12} \text{ erg cm}^{-2} \text{ s}^{-1}$ and $4.17 \cdot 10^{-12} \text{ erg cm}^{-2} \text{ s}^{-1}$. The bolometric luminosities of the eclipsing binary components were evaluated as $\log L_{\text{bol}}/L_{\odot} = 5.383$ and 5.102 , whilst the third light contribution was found to be near 40% of the total light of the triple system (Ibanoglu et al. 2013). Evaluating the sum of these bolometric luminosities, assuming a 2 kpc distance and comparing with the above X-ray fluxes corrected for the interstellar absorption results in $\frac{L_{\text{X}}}{L_{\text{bol}}}$ between $3.8 \cdot 10^{-7}$ and $5.7 \cdot 10^{-7}$. Using instead the typical bolometric magnitudes as quoted by Martins et al. (2005) for stars of equal spectral types yields $\frac{L_{\text{X}}}{L_{\text{bol}}}$ between $2.0 \cdot 10^{-7}$ and $3.1 \cdot 10^{-7}$. HD 167971 thus appears mildly overluminous in X-rays compared to the canonical $L_{\text{X}}/L_{\text{bol}}$ relation.

Figure 4 displays the variations in the X-ray flux as a function of the orbital phase of the tertiary component (left panel) and of the orbit of the inner eclipsing binary (right panel). The observed X-ray emission of HD 167971 is a combination of (i) the intrinsic emission of the three components of this triple system, (ii) a possible contribution from the wind interaction zone of the short-period binary, and (iii) the collision between the combined winds of the inner binary and the wind of the third component. The third of these contributions is expected to undergo a $1/r$ modulation similar to the one observed for HD 168112. However, Fig. 4 unveils very little coherent variations with the phase of the outer orbit. This could primarily be due to the rather scarce phase coverage. Indeed, existing *XMM-Newton* data only sample phases ϕ_{outer} around 0.3 and 0.7. Because these phases are roughly symmetrical with respect to periastron ($\phi_{\text{outer}} = 0.0$) and correspond to separations differing by only a few percent, the $1/r$ values are very similar and the ensuing X-ray emissions should thus display a similar level, as observed. By far, the largest variations in

the X-ray emission from the outer colliding wind interaction are expected around periastron, but such data are currently lacking. The data points collected around $\phi_{\text{outer}} = 0.7$ display significant variations, but this variability occurs with a timescale that is too short to be due to a $1/r$ modulation. The right panel of Fig. 4 shows instead that these variations probably arise on the timescale of the inner orbit. Indeed, the existing data suggest a modulation that is reminiscent of eclipses in the inner binary (see Fig. 5). This is especially true for the soft and medium energy bands, whilst the variations in the hard band are more erratic. In the medium energy band, the variations have peak-to-peak amplitudes of 40%.

The part of HD 167971’s X-ray emission that undergoes a short-term modulation consistent with the orbital period of the inner eclipsing binary must therefore arise inside this short period binary. There are three possibilities to explain the origin of this emission:

- It could arise from the intrinsic emission due to wind-embedded shocks (Feldmeier et al. 1997). The modulation of the X-ray flux would then result from eclipses by the stars and their winds, as was suggested, for instance, for the case of 29 CMa (Berghöfer & Schmitt 1995). Observationally, the intrinsic emission of O-type stars typically amounts to $10^{-7} L_{\text{bol}}$ and is mostly soft with $kT \sim 0.6 \text{ keV}$ (e.g. Berghöfer et al. 1996; Nazé 2009). Based on the spectral types proposed by Maíz Apellániz et al. (2019), and the calibration of Martins et al. (2005), we estimate $\log(L_{\text{bol}}/L_{\odot}) \simeq 5.91$ for the primary and $\log(L_{\text{bol}}/L_{\odot}) \simeq 5.69$ for the secondary component. Assuming a distance of 2 kpc, the X-ray flux due to wind-embedded shocks is estimated as $\sim 6.5 \cdot 10^{-13} \text{ erg s}^{-1} \text{ cm}^{-2}$ for the primary and $\sim 3.9 \cdot 10^{-13} \text{ erg s}^{-1} \text{ cm}^{-2}$ for the secondary. Each star contributes a non-negligible fraction ($\sim 15\%$ and $\sim 9\%$ respectively for the primary and secondary star) of the maximum total ISM-corrected X-ray emission, but these contributions

fall short by about a factor of 2 to 4 compared to what is needed to explain the observed $\sim 40\%$ peak to peak variations by occultation and eclipse effects.

- It could arise from a wind interaction between the components of the inner binary. Indeed, short-period massive binaries may display a phase shift in their X-ray light curve with respect to the optical light curve. This is due to the Coriolis deflection of the wind interaction region (e.g. V444 Cyg, $P_{\text{orb}} = 4.21$ d, Lomax et al. 2015; WR 21 and WR 31, $P_{\text{orb}} = 8.25$ d and 4.83 d, Nazé et al. 2023). De Becker (2015) argued that because of the radiative nature of the wind interaction in the inner binary, the total X-ray emission of HD 167971 should be dominated by this contribution. However, from the observational viewpoint, wind interactions in such short-period O-star binaries are often X-ray faint (e.g. 29 CMa; Berghöfer & Schmitt 1995, and HD 149404, Rauw et al. 2024). From a theoretical viewpoint, radiative wind interaction zones are expected to be subject to thin shell instabilities that considerably lower their X-ray emission (Stevens et al. 1992; Kee et al. 2014). The problem would be even worse if the inner eclipsing binary is in an overcontact configuration as suggested by Mayer et al. (2010) and Ibanoglu et al. (2013) based on their photometric light curve analyses. In such cases, the strong head-on collision of the winds along the line of centres is lacking and the wind interaction region has an annular shape, which would make it less prone to eclipsing effects (Montes et al. 2013). Whilst we cannot rule out the colliding winds as the origin of the emission, a full hydrodynamic modelling of the wind interaction is probably needed to assess the plausibility of this scenario.
- It could form in a magnetically confined wind of one of the components of the inner binary. In magnetic massive stars, the mostly dipolar magnetic field channels the wind material towards the magnetic equator where the flows from the two hemispheres collide, leading thereby to an enhanced X-ray emission (for a review see ud-Doula & Nazé 2016). The eclipse of such a magnetically confined wind by the companion star could indeed lead to a modulation of the observed X-ray emission. Hubrig et al. (2023) reported the detection of a strong (1324 ± 582 G) longitudinal magnetic field in one of the components of the eclipsing binary. However, given the large error bar, this 2.3σ detection requires confirmation. We note that Neiner et al. (2015) had previously analysed the same observation, reporting a non-detection. Again, more evidence needs to be gathered to check the validity of this scenario.

Whilst the above discussion highlights the fact that the X-ray emission of HD 167971 arises from several regions, one obviously expects a contribution coming from the interaction between the winds of the inner binary and the wind of the tertiary component. In fact, the non-thermal radio emission of this system is clearly ruled by the outer orbit (Blomme et al. 2007), pointing towards an energetic wind-wind collision. Blomme et al. (2007) estimated that the tertiary star was at its closest position to the inner binary in 1988 in good agreement with the ephemerides of Le Bouquin et al. (2017)⁵. Sanchez-Bermudez et al. (2019) discussed two very long baseline interferometry (VLBI) observations in 2006 and 2016. These data unveiled a

⁵ This is also confirmed by the EVN radio data of De Becker et al. (2024) that were collected near apastron of the tertiary component at a time when the synchrotron emission of this system was at a low level. The radio emission of HD 167971 remained unresolved in this observation.

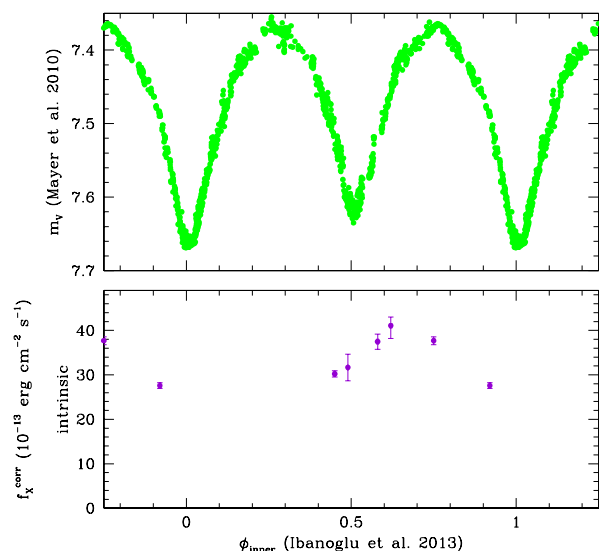


Fig. 5. Comparison between optical and X-ray light curve of HD 167971. Top panel: V-band photometry of HD 167971 (Mayer et al. 2010) folded with the ephemerides of the inner eclipsing binary. Bottom panel: X-ray flux in the 0.5 keV – 10 keV band corrected for the interstellar absorption and folded with the ephemerides from Ibanoglu et al. (2013). We note that the uncertainties on the ϕ_{inner} of the X-ray data are smaller than the size of the symbols. They range between $1.6 \cdot 10^{-3}$ for the oldest data and $2.8 \cdot 10^{-3}$ for the most recent observation.

change in orientation of the elongated emission region, consistent with the orbital motion of the tertiary component. These results demonstrate that the non-thermal radio emission from HD 167971 arises from the wind-wind collision between the inner eclipsing binary and the tertiary component. The location of the emitting region between the positions of the inner binary and the tertiary further indicates that the combined wind of the inner binary is stronger than the wind of the tertiary star. The next periastron passage of the tertiary component should take place in 2030. From the 0.44 ± 0.02 eccentricity derived by Le Bouquin et al. (2017), one can then estimate that the contribution of the outer colliding wind interaction should increase by more than a factor of 2 between the existing data around $\phi_{\text{outer}} \approx 0.3$ or ≈ 0.7 and periastron if there is no impact of shock modification.

The VLBI data of Sanchez-Bermudez et al. (2019) yielded a radio spectral index of $\alpha = -1.1$, significantly steeper than expected for synchrotron emission in an optically thin environment ($\alpha = -0.5$). Sanchez-Bermudez et al. (2019) interpreted this as a consequence of efficient IC cooling leading to a softening of the electron energy spectrum or as a consequence of modified shocks. Whilst the current sampling of the outer orbit is insufficient to search for evidence for or against shock modification, we tried to look for evidence of non-thermal X-ray emission arising from the IC scattering by the relativistic electrons. As for HD 168112, we repeated the fits of a model including beside a 2-T thermal plasma a power-law component with Γ fixed to 1.5. These fits were again of poorer quality than those described in Sect. 3.2.2. The normalisation of the power-law was only significant at the $\sim 3.5\sigma$ level. The intrinsic flux in the 0.5 keV – 10 keV band of the power-law component would be typically of order $4 \cdot 10^{-13}$ erg cm⁻² s⁻¹, corresponding to $\sim 3\%$ of the total ISM-corrected X-ray flux. We stress that these models failed to reproduce the Fe xxv line at 6.7 keV clearly seen in the EPIC-pn spectrum from observation 3. Hence, as in the

case of HD 168112, we conclude that the flux quoted for the non-thermal X-ray emission must be seen as a strict upper limit and that currently, there is no detection of a genuine non-thermal high-energy emission in HD 167971.

5. Conclusions

In this study we used a new set of *XMM-Newton* observations to gain further insight into the X-ray properties of two colliding wind systems that are well-known non-thermal radio emitters. Taking advantage of the orbital elements that were recently established for HD 168112, we find that the X-ray spectra of this highly eccentric 1.4 yr binary unveil a clear phase-dependent X-ray over-luminosity. The X-ray fluxes display variability consistent with the expected $1/r$ modulation for an adiabatic wind interaction. We show that the shocks remain adiabatic at periastron and do not collapse, unlike what has been observed in other eccentric massive binaries. Despite the presence of a population of relativistic electrons, as revealed by the synchrotron radio emission, we find no evidence of a significant shock modification due to the action of these relativistic electrons. We also failed to detect any clear indication of a non-thermal X-ray emission that could arise from IC scattering by relativistic electrons. Our analysis indicates that wind-embedded shocks in the individual winds of the binary contribute between 38% and 81% of the X-ray flux at periastron and apastron, respectively.

The existing X-ray data of the triple system HD 167971 were not sufficient to look for a $1/r$ modulation locked to the orbit of the tertiary component. This is mostly because observations of the outer orbit near periastron are still missing. From the current best knowledge of the outer orbit, the next opportunity to fill this gap is expected around 2030. Meanwhile, the existing data hint at a modulation of the X-ray emission on the orbital period of the inner eclipsing binary. This suggests that a significant fraction of the observed X-ray emission must arise inside this inner binary, although its exact origin remains uncertain. Whilst the emission from wind-embedded shocks is probably not sufficient to explain the observed modulation, colliding winds possibly coupled with a magnetically confined wind of one of the components of the inner binary could provide an explanation. However, a better sampling of the inner orbital cycle would be needed to determine the constraints needed to guide future models of this system.

Acknowledgements. The Liège team acknowledges support from the Fonds National de la Recherche Scientifique (Belgium) and the Belgian Federal Science Policy Office (BELSPO) in the framework of the PRODEX Programme (HER-MeS contract). ADS and CDS were used for this research.

References

Abbott, D.C., Biegging, J.H., & Churchwell, E.B. 1984, *ApJ*, 280, 671
 Arnaud, K.A. 1996, in *Astronomical Data Analysis Software and Systems V*, eds. G. Jacoby & J. Barnes, ASP Conf. Series, 101, 17
 Asplund, M., Grevesse, N., Sauval, A.J., & Scott, P. 2009, *ARA&A*, 47, 481
 Berghöfer, T.W., Schmitt, J.H.M.M., & Cassinelli, J.P. 1996, *A&AS*, 118, 481
 Berghöfer, T.W., & Schmitt, J.H.M.M. 1995, in *Wolf-Rayet stars: Binaries, Colliding Winds, Evolution*, eds. K.A. van der Hucht & P.M. Williams, Proc. IAU Symp. 163, Kluwer Academic Publisher, Dordrecht, 382
 Biegging, J.H., Abbott, D.C., & Churchwell, E.B. 1989, *ApJ*, 340, 518
 Blomme, R., van Loo, S., De Becker, M., et al. 2005, *A&A*, 436, 1033
 Blomme, R., De Becker, M., Runacres, M.C., Van Loo, S., & Setia Gunawan, D.Y.A. 2007, *A&A*, 464, 701
 Blomme, R., Nazé, Y., Volpi, D., et al. 2013, *A&A*, 550, A90
 Blomme, R., Rauw, G., Volpi, D., Nazé, Y., & Abdul-Masih, M. 2024 *A&A*, in press, arXiv:2405.03247
 Bohlin, R.C., Savage, B.D., & Drake, J.F. 1978, *ApJ*, 224, 132
 Chen, W., & White, R.L. 1991, *ApJ*, 366, 512

Davidge, T.J., & Forbes, D. 1988, *MNRAS*, 235, 797
 De Becker, M. 2015, *MNRAS*, 451, 1070
 De Becker, M., Rauw, G., Blomme, R., et al. 2004, *A&A*, 420, 1061
 De Becker, M., Rauw, G., Blomme, R., et al. 2005, *A&A*, 437, 1029
 De Becker, M., Sana, H., Absil, O., Le Bouquin, J.-B., & Blomme, R. 2012, *MNRAS*, 423, 2711
 De Becker, M., Marcote, B., Furst, T., & Benaglia, P. 2024, *A&A*, 682, A160
 den Herder, J.W., Brinkman, A.C., Kahn, S.M., et al. 2001, *A&A*, 365, L7
 Dougherty, S.M., & Williams, P.M. 2000, *MNRAS*, 319, 1005
 Farnier, C., Walter, R., & Leyder, J.-C. 2011, *A&A*, 526, A57
 Feldmeier, A., Puls, J., & Pauldrach, A.W.A. 1997, *A&A*, 322, 878
 Gayley, K.G., Owocki, S.P., & Cranmer, S.R. 1997, *ApJ*, 475, 786
 Gosset, E., & Nazé, Y. 2016, *A&A*, 590, A113
 Gudennavar, S.B., Bubbly, S.G., Preethi, K., & Murthy, J. 2012, *ApJS*, 199, 8
 Hamaguchi, K., Corcoran, M.F., Pittard, J.M., et al. 2018, *Nature Astronomy*, 2, 731
 Hubrig, S., Järvinen, S.P., Ilyin, I., Schöller, M., & Jayaraman, R. 2023, *MNRAS*, 521, 6228
 Ibanoglu, C., Çakırlı, Ö., & Sipahi, E. 2013, *MNRAS*, 436, 750
 Jansen, F., Lumb, D., Altieri, B., et al. 2001, *A&A*, 365, L1
 Kee, N.D., Owocki, S.P., & ud-Doula, A. 2014, *MNRAS*, 438, 3557
 Le Bouquin, J.-B., Sana, H., Gosset, E., et al. 2017, *A&A*, 601, A34
 Leitherer, C., Forbes, D., Gilmore, A.C., et al. 1987, *A&A*, 185, 121
 Leyder, J.-C., Walter, R., & Rauw, G. 2010, *A&A*, 524, A59
 Lomax, J.R., Nazé, Y., Hoffman, J.L., et al. 2015, *A&A*, 573, A43
 Mackey, J., Jones, T.A.K., Brose, R., et al. 2023, *MNRAS*, 526, 3099
 Maíz Apellániz, J., Trigueros Páez, E., Negueruela, I., et al. 2019, *A&A*, 626, A20
 Martins, F., Schaerer, D., & Hillier, D.J. 2005, *A&A*, 436, 1049
 Mayer, P., Božić, H., Lorenz, R., & Drechsel, H. 2010, *Astron. Nachr.* 331, 274
 Montes, G., Ramirez-Ruiz, E., De Colle, F., & Strickler, R. 2013, *ApJ*, 777, 129
 Mossoux, E., Pittard, J.M., Rauw, G., & Nazé, Y. 2020, *A&A*, 636, A109
 Muijres, L.E., Vink, J.S., de Koter, A., Müller, P.E., & Langer, N. 2012, *A&A*, 537, A37
 Nazé, Y. 2009, *A&A*, 506, 1055
 Nazé, Y., Damerdjı, Y., Rauw, G., et al. 2010, *ApJ*, 719, 634
 Nazé, Y., Mahy, L., Damerdjı, Y., et al. 2012, *A&A*, 546, A37
 Nazé, Y., Rauw, G., Johnson, R., Gosset, E., & Hoffman, J.L. 2023, *MNRAS*, 526, 2167
 Neiner, C., Grunhut, J., Leroy, B., De Becker, M., & Rauw, G. 2015, *A&A*, 575, A66
 Pandey, J.C., Pandey, S.B., & Karmakar, S. 2014, *ApJ*, 788, 84
 Pittard, J.M., & Dawson, B. 2018, *MNRAS*, 477, 5640
 Pittard, J.M., & Dougherty, S.M. 2006, *MNRAS*, 372, 801
 Pittard, J.M., Romero, G.E., & Vila, G.S. 2021, *MNRAS*, 504, 4204
 Putkuri, C., Gamen, R., Morrell, N.I., et al. 2023, *MNRAS*, 525, 6084
 Rauw, G. 2022, in *Handbook of X-ray and Gamma-ray Astrophysics*, eds. C. Bambi & A. Santangelo, Springer Living Reference Work, id.108
 Rauw, G., & Nazé, Y. 2016, *AdSpR*, 58, 761
 Rauw, G., Blomme, R., Waldron, W.L., et al. 2002, *A&A*, 394, 993
 Rauw, G., Blomme, R., Nazé, Y., et al. 2016, *A&A*, 589, A121
 Rauw, G., Lizin, S., Rosu, S., & Mossoux, E. 2024, *A&A*, 686, A152
 Reipurth, B. 2008, in *Handbook of Star Forming Regions*, Vol. II, *Astronomical Society of the Pacific*, ed. B. Reipurth
 Reitberger, K., Kissmann, R., Reimer, A., Reimer, O., & Dubus, G. 2014, *ApJ*, 782, 96
 Reitberger, K., Reimer, A., Reimer, O., & Takahashi, H. 2015, *A&A*, 577, A100
 Sana, H., de Mink, S.E., de Koter, A., et al. 2012, *Science*, 337, 444
 Sana, H., Le Bouquin, J.-B., Lacour, S., et al. 2014, *ApJS*, 215, 15
 Sanchez-Bermudez, J., Alberdi, A., Schödel, R., et al. 2019, *A&A*, 624, A55
 Smith, R.K., & Brickhouse, N.S. 2001, *ApJ*, 556, L91
 Stevens, I.R., & Pollock, A.M.T. 1994, *MNRAS*, 269, 226
 Stevens, I.R., Blondin, J.M., & Pollock, A.M.T. 1992, *ApJ*, 386, 265
 Strüder, L., Briel, U., Dennerl, K., et al. 2001, *A&A*, 365, L18
 Turner, M.J.L., Abbey, A., Arnaud, M., et al. 2001, *A&A*, 365, L27
 ud-Doula, A., & Nazé, Y. 2016, *AdSpR*, 58, 680
 van Loo, S., Runacres, M.C., & Blomme, R. 2005, *A&A*, 433, 313
 Vink, J.S. 2022, *ARA&A*, 60, 203
 Wilms, J., Allen, A., & McCray, R. 2000, *ApJ*, 542, 914
 Wright, A.E., & Barlow, M.J. 1975, *MNRAS*, 170, 41
 Zhekov, S.A. 2021, *MNRAS*, 500, 4837